metals

MDPI

Article

Warm Deformation at the (α + γ) Dual-Phase Region to Fabricate 2 GPa Ultrafine-Grained TRIP Steels

Jinxuan Zhao [1,†], Hai Wang [2,†], Konrad Koenigsmann [3], Xianzhe Ran [4], Peng Zhang [2], Shuyuan Zhang [2], Yi Li [2,5], Huan Liu [2,5], Hui Liu [5], Ling Ren [2,6,*], Hui Yao [1,*] and Ke Yang [2]

[1] College of Science, Shenyang University of Chemical Technology, 11# Street Shenyang Economic & Technology Development Area, Shenyang 110142, China; 2022127@stu.syuct.edu.cn
[2] Shi-Changxu Innovation Center for Advanced Materials, Institute of Metal Research, Chinese Academy of Sciences, Shenyang 110016, China; hwang13s@imr.ac.cn (H.W.); pengzhang@imr.ac.cn (P.Z.); zhangsy@imr.ac.cn (S.Z.); yli20b@imr.ac.cn (Y.L.); hliu18s@imr.ac.cn (H.L.); kyang@imr.ac.cn (K.Y.)
[3] Faculty of Physics, University of Chicago, Chicago, IL 60637, USA
[4] Research Institute of Frontier Science, Beihang University, 37 Xueyuan Road, Beijing 100191, China; rxianzhe@buaa.edu.cn
[5] School of Materials Science and Engineering, University of Science and Technology of China, Shenyang 110016, China; hliu17b@imr.ac.cn
[6] Binzhou Institute of Technology, Shandong Key Laboratory of Advanced Aluminium Materials and Technology, Weiqiao-UCAS Science and Technology Park, Binzhou 256606, China
* Correspondence: lren@imr.ac.cn (L.R.); yaohui@syuct.edu.cn (H.Y.)
† These authors contributed equally to this work.

Abstract: Transformation-Induced Plasticity (TRIP) steels have a range of applications in the vehicle engineering field. Developing TRIP steels with improved mechanical properties would not only allow for lightweight designs, but would also improve the safety of the materials in service. In this study, we report novel 0.4C-(3, 5, 7)Mn-1.2Mo-0.8V TRIP steels; these steels were melted and then warm-deformed at the (α + γ) dual-phase region to fabricate ultrafine-grained microstructures with average grain sizes of 200–500 nm. Results show that the tensile strengths of the steels range between 1.9 and 2.1 GPa, and their elongations range between 7% and 8.5%. The microstructural thermostability of the steels gradually decreases with an increase in the manganese content. Compared with conventional TRIP steels fabricated using the cold-rolling and annealing method, the warm-deformed TRIP steels presented here can prevent cracks forming during the fabrication process. More importantly, these steels have significantly lower dislocation densities, thus improving their ductility. The present research results provide new ideas for the design of future ultrahigh-strength TRIP steels.

Keywords: TRIP steel; ultrafine-grained; warm deformation; 2 GPa; medium manganese steel

check for updates

Citation: Zhao, J.; Wang, H.; Koenigsmann, K.; Ran, X.; Zhang, P.; Zhang, S.; Li, Y.; Liu, H.; Liu, H.; Ren, L.; et al. Warm Deformation at the (α + γ) Dual-Phase Region to Fabricate 2 GPa Ultrafine-Grained TRIP Steels. *Metals* **2023**, *13*, 1997. https://doi.org/10.3390/met13121997

Academic Editor: Saeed Sadeghpour

Received: 16 November 2023
Revised: 4 December 2023
Accepted: 7 December 2023
Published: 12 December 2023

1. Introduction

TRIP steels are widely used in the vehicle engineering field [1,2]. Currently, the most common processing procedure for manufacturing high-strength TRIP steels is hot rolling, followed by cold rolling, and finally annealing. The as-prepared microstructure is normally composed of ferrite and austenite [3–6]. When a load is applied to the material, the material exhibits good plastic deformation due to the soft ferrite, while the austenite can transform into hard martensite, which suppresses necking in the soft microstructure region. Therefore, TRIP steels usually have excellent comprehensive mechanical properties [1,2,7,8]. The development of novel higher-strength TRIP steels is of great importance for future lightweight designs and for improving the safety of the materials in service.

For this purpose, Wang et al. optimized the hot-rolling and cold-rolling parameters of a low-alloyed TRIP steel and fabricated a lamellar microstructure to improve the stability of the retaining austenite. The tensile strength of the steel was improved to 1.2 GPa, and the elongation was as high as 25% [9]. Qichun Peng et al. developed a 0.12C-5Mn-1Al steel which was subjected to cold rolling then quenching and tempering; excellent mechanical properties with a strength of 878~1373 MPa and ductility of 18~40% were achieved [10]. Aleksandra Kozłowska et al. fabricated a bainite TRIP steel; static tensile tests which were carried out at −60 to 200°C showed that the tensile strength was in a range of 1320~1440 MPa, and the elongation was 9~12% [11]. Li et al. developed a unique cold-rolling technology to increase the stacking fault energy of a 0.31C-11.7Mn-1.1Al medium manganese steel. The strength of the alloy increased to nearly 1.5 GPa; however, the elongation decreased to 12.5% [12]. Huang et al. designed a cold deformation and partitioning TRIP steel. Though the tensile strength of the steel further increased to 1.9 GPa, its ductility decreased significantly [13]. Gao et al. prepared a high-dislocation-density 0.19C-1.01Mn-1.46Si TRIP steel using low-temperature severe plastic deformation [14]. The tensile strength of the material was higher than 2.1 GPa; however, its elongation was only 3%. It can be seen that although the cold-rolling method can be used to fabricate ultrahigh-strength TRIP steels, the applications of these steels are limited for two important reasons: First, as the strength of the TRIP steels increases, cold rolling might not only damage the rollers, but also lead to the formation of cracks in the steel [3–6]. Second, the high dislocation densities of steels fabricated using cold rolling might decrease the mobility of dislocations, thus significantly decreasing the ductility of the steels [12–15].

The aim of the present study is to address the two issues noted above. Novel 0.4C-(3, 5, 7)Mn-1.2Mo-0.8V TRIP steels were designed for this purpose. These steels were melted and then warm-deformed at the (α + γ) dual-phase region so as to fabricate ultrafine-grained and ultrahigh-strength TRIP steels. Then, both the mechanical properties and microstructural thermostability of the steels were evaluated. Compared with conventional TRIP steels that are manufactured using cold rolling and annealing, the warm-deformed steels not only exhibit decreased deformation flow stress, thus preventing the formation of cracks, but also have lower dislocation densities, thus improving the ductility of the materials. These experimental results will provide new ideas for the development of future ultrahigh-strength TRIP steels.

2. Experimental Procedure

A 25 kg vacuum induction melting furnace (ALD Vacuum Technologies, Frankfurt, Germany) was used to melt ingots of the 0.4C-(3, 5, 7)Mn-1.2Mo-0.8V steels, hereafter referred to as the 3Mn, 5Mn, and 7Mn steels, respectively. A piece of material was sectioned from the top of each ingot, then φ3 × 2 mm and φ8 × 12 mm cylindrical samples were machined. A SETSYS-18/HPR20 (Netzsch, Munich, Germany) differential thermal analyzer (DTA) was used to measure the phase transformation temperature of the φ3 × 2 mm cylindrical samples. The heating and cooling rates were both 1 °C/s in the DTA tests. A Gleeble 3800 thermal simulation machine (DSI, Berlin, Germany) was used to perform hot compression experiments on the φ8 × 12 mm cylindrical samples. The test strain rate was 0.2 s^{-1} and the height reduction was 70% (corresponding to a true strain of 1.2). Following these tests, the ingots of the three steels were forged using a 2000-ton hydraulic press machine. First, the ingots were forged into φ70 × 140 mm cylindrical billets at 1200 °C. Subsequently, for the φ70 × 140 mm cylindrical billets of 3Mn, 5Mn and 7Mn steels, they were held at 700 °C, 670 °C and 640 °C for 2 h, respectively. Finally, they were forged into φ220 × 14 mm plates at the same temperatures. After forging, they were air cooled to room temperature (Figure 1). Tensile specimens which conformed to the ASTM E8/E8M-16a standard with a diameter of 5 mm and a gauge length of 25 mm were machined from the central part of as-forged plates.

An INSTRON 5982 universal electronic tensile testing machine (INSTRON, Norwood, MA, USA) was used to measure the room temperature tensile properties of the as-forged steels with a test strain rate of 0.001 s^{-1}. The tensile properties of the steels were given by the averages of three parallel experiments. A MERLIN Compact (Zeiss, Jenoptik, Germany) field emission scanning electron microscope (SEM) equipped with an electron backscattered diffraction (EBSD) detector was used to characterize the microstructures of the steels both before and after the tensile tests. The acceleration voltage for the EBSD tests was 25 kV, the current was 18 nA, the scanning step size was 20 nm, and the lowest test resolution was above 80%. Channel 5.0 software was used to analyze the acquired data. A TalosF200x (FEI, Hillsboro, OR, USA) transmission electron microscope (TEM) was also used to characterize the microstructures of the three steels. The samples for TEM observations were first mechanically thinned to 50 μm and were then electrolytically polished with a twin-jet thinner using a solution of 10 vol.%$HClO_4$ + 90 vol.% C_2H_5OH at 25 V and −25 °C. The microstructural thermostability of the ultrafine-grained steels was evaluated by means of thermal exposure experiments. The as-forged steels were machined to six 10 mm × 10 mm × 10 mm cubic samples, then each steel was exposed at 100 °C, 200 °C, 300 °C, 400 °C, 500 °C, and 600 °C for 1 h, respectively. Each sample surface was grinded and polished, then an LM247AT Micro-Vickers sclerometer (LECO, St. Joseph, MO, USA) was used to measure the hardness. The tested load was 5.88 N and the loading time was 5 s. At the surface of each sample, measurements were conducted five times at different regions.

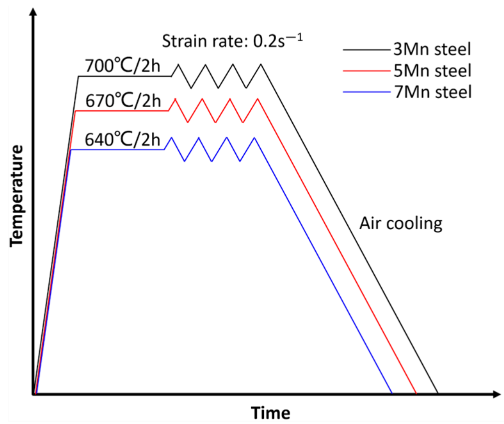

Figure 1. A schematic diagram of the forging processes of three experimental steels.

3. Results and Discussion

3.1. Phase Transformation Temperatures of Three Experimental Steels

Figure 2 shows the DTA curves of the three steels being investigated. The black and red curves correspond to the heating and cooling processes of the materials, respectively. During the heating process, ferrite transforms into austenite, which is an endothermic process. Therefore, the Ac1 and Ac3 temperatures can be determined by finding the starting and ending temperatures of the endothermic dip. The Ac1 temperatures of the 3Mn, 5Mn, and 7Mn steels were measured to be 686 °C, 650 °C, and 638 °C, respectively. The Ac3 temperatures were determined to be 713 °C, 703 °C, and 687 °C, respectively. It can be seen that both the Ac1 and Ac3 temperatures decrease as the manganese content increases. This is due to the fact that manganese is an austenite-stabilizing element, meaning it can enlarge the austenite zone [16]. During the cooling process, supercooled austenite transforms into martensite, which is an exothermic process. Therefore, the Ms temperature can be determined by finding the starting temperature of the exothermic peak. The Ms temperatures of the 3Mn, 5Mn, and 7Mn steels were measured to be 287 °C, 213 °C, and 131 °C, respectively. It can be seen that for every 1 wt.% increase in manganese in the steel, the Ms temperature of the steel decreases by about 40 °C, which is consistent with the results from the literature [2,17].

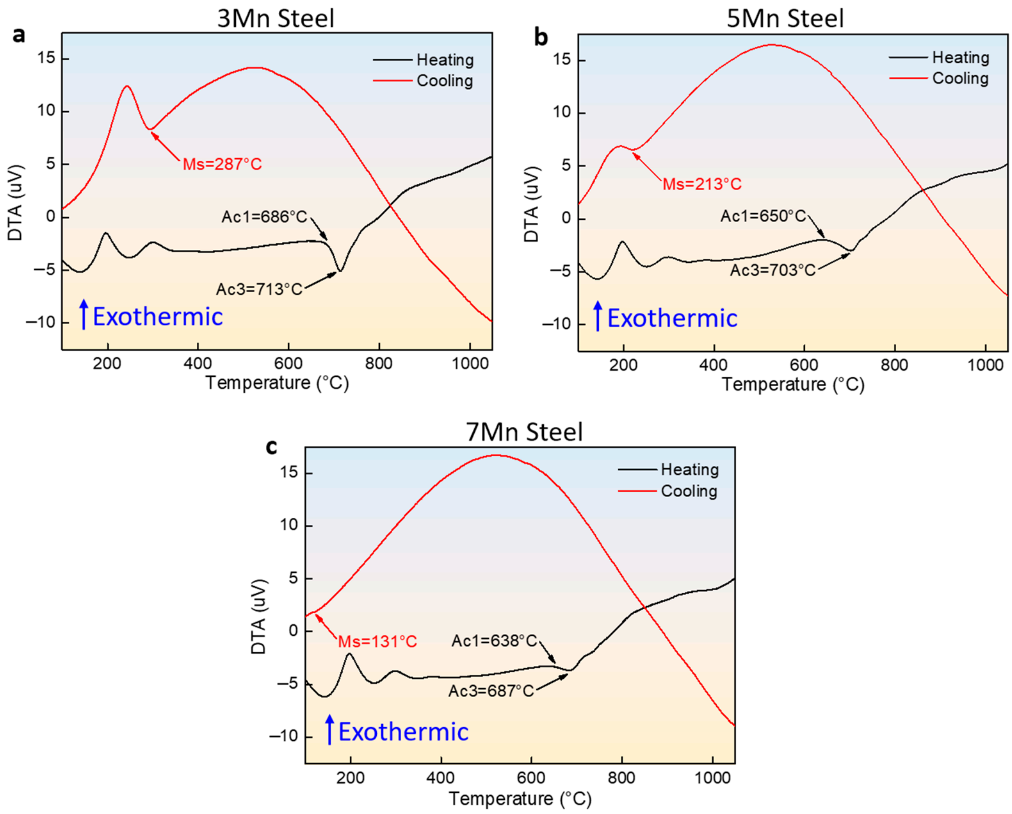

Figure 2. DTA–temperature curves of three experimental steels during heating and cooling periods: (**a**) 3Mn steel; (**b**) 5Mn steel; (**c**) 7Mn steel.

3.2. Flow Behaviors of Three Steels during Hot Compressive Tests

According to the measured Ac1 and Ac3 temperatures of the three steels, they were hot-compressed at temperatures around their ($\alpha + \gamma$) dual-phase region so as to investigate their flow stresses and to investigate the possibility of fabricating ultrafine-grained TRIP steels using warm deformation. Hot compressive stress-strain curves of three steels were shown in Figure 3. It can be seen that each curve can be divided into three parts: (1) the strain-hardening period; (2) the strain-softening period; and (3) the steady-state flow period [18]. During the first period ($0 \leq \varepsilon \leq 0.05$), the flow stress rapidly increased with the increase in the strain, which is due to the fact that the dislocation source in the steel was activated by the deformation strain and the multiplication of dislocations, resulting in dislocation strengthening. During the second period ($0.05 \leq \varepsilon \leq 0.8$), the flow stress decreased with the increase in the strain, which is due to the role of dynamic recrystallization that would consume dislocations in the steel, thus giving rise to softening [19]. During the third period ($\varepsilon > 0.8$), the flow stress barely changed with the increase in the strain, which is due to the role of dislocation strengthening and dynamic recrystallization softening, to achieve a dynamic balance state. Furthermore, for each material, flow stress always increases as the deformation temperature decreases. When deformed at a fixed temperature, the flow stress increases as the manganese content increases. This is because the austenite volume fraction increases as the manganese content increases, and because austenite has a higher creep strength than ferrite during warm deformations [20]. It is worth mentioning that although the peak flow stresses of the present steels are 500–750 MPa, they are much lower than the peak flow stresses of conventional TRIP steels, which exhibit peak flow stresses ranging from 1000–2000 MPa [3–6]. Therefore, the present manufacturing method would alleviate the abrasion of dies and prevent crack formation during the fabrication process of TRIP steels.

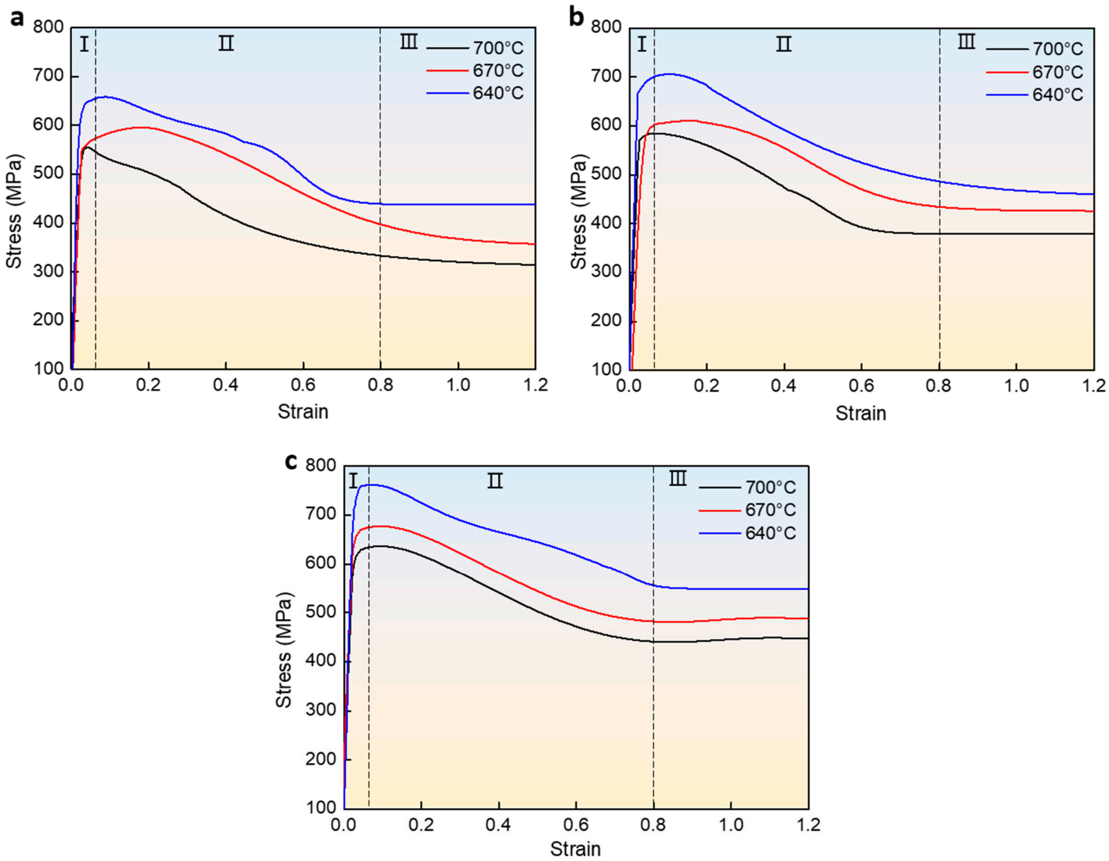

Figure 3. Hot compressive stress-strain curves of three experimental steels at 640~700 °C: (**a**) 3Mn steel; (**b**) 5Mn steel; (**c**) 7Mn steel.

3.3. As-Forged Microstructure Characterization of Three Steels

Based on the hot compressive experiments above, hot forging was conducted at the same temperature and deformation strain rate. Figure 4 shows the EBSD and TEM characterizations of the as-forged microstructures of the 3Mn, 5Mn, and 7Mn steels at 700 °C, 670 °C, and 640 °C, respectively. Taken together with the results shown in Figure 2a–c, it can be seen that for each steel, the warm-forged temperature is just in the ($\alpha + \gamma$) dual-phase region. All three steels can obtain ultrafine-grained microstructures with average α grain sizes of 200–500 nm after warm forging. This is because when the steels are deformed at the dual-phase region, the grain growth of the α phase is constrained by the γ phase. Similarly, the grain growth of the γ phase is constrained by the α phase. In the phase distribution maps (PDMs) in Figure 4, the blue areas correspond to the α phase, and the red areas correspond to the γ phase. It can be seen that the area fraction of the γ phase increases as the manganese content increases. There are three reasons for this. First, increasing the manganese content can significantly decrease the Ms temperature of the steels (Figure 2). Second, manganese can diffuse from the α phase to the γ phase during warm deformation, and when the manganese content in the γ phase exceeds 10–12 wt.% [21], the Ms temperature can fall below room temperature. Third, the experimental steels contain a high content of Mo, which increases the hardenability of the steel and suppresses the γ phase transforming into the pearlite in the air-cooling process after forging. Hence, the metastable γ phase can be retained at room temperature. In the inverse pole figures (IPFs) in Figure 4, the blue areas correspond to {111} planes that are perpendicular to the forging direction (FD); the red areas correspond to {001} planes that are perpendicular to the FD; and the green areas correspond to {101} planes that are perpendicular to the FD. Since the different colors are homogenously distributed in the IPF maps, it can be seen that there is no preferred orientation in the three steels. In the TEMs in Figure 4, numerous dislocations can be seen inside the three materials; however, the dislocation densities are much lower than in conventional TRIP steels fabricated using cold deformation [12–14]. This should be the result of dislocation annihilation during warm deformation.

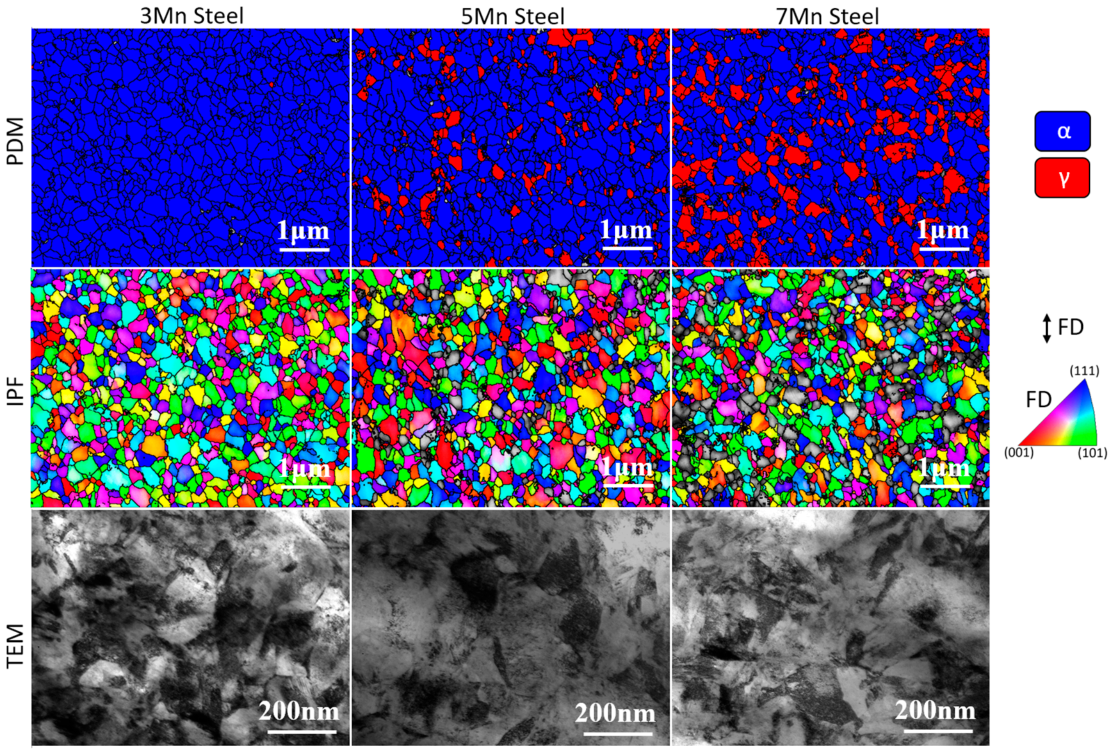

Figure 4. The effect of manganese content on the as-forged microstructure. The forging direction (FD) is shown on the right. Both phase distribution maps (PDMs) and inverse pole figure orientation maps (IPFs) indicate that all three steels possess ultrafine-grained microstructures.

Figure 5 shows grain size distribution maps of the α phase in the three experimental steels, which are calculated by means of EBSD analysis software Channel 5.0. In the 3Mn steel, 26% of α grains have a grain size below 100 nm, and the average α grain size of the steel is 473 nm. In the 5Mn steel, 36% of α grains have a grain size below 100 nm, and the average α grain size of the steel is 447 nm. In the 7Mn steel, 43% of α grains have a grain size below 100 nm, and the average α grain size of the steel is 338 nm. Hence, it can be seen that the experimental steels are sorted into 3Mn steel, 5Mn steel and 7Mn steels by descending order of grain size. This is due to the fact that the forging temperatures of the steels are 700 °C, 670 °C and 640 °C, respectively. A decreasing forging temperature is beneficial for suppressing grain coarsening during the warm deformation process.

To further analyze the preferential orientation of the α phase in as-forged steels, the 3Mn steel was taken as an example, and the orientation distribution function (ODF) maps were calculated as shown in Figure 6. Our hypothesis was that the benchmark α grain has a crystallographic orientation of [001], [010], [100] directions, parallel with the forging direction and two other perpendicular radial directions, respectively. Through first rotating the benchmark α grain along its [001] axis to the angle of Φ1, then rotating along its [100] axis to the angle of Φ, and finally rotating along its [001] axis again to the angle of Φ2, an α grain with the arbitrary crystallographic orientation can be obtained. Therefore, the Euler angle (Φ1, Φ, Φ2) can be used to express the orientation of an α grain. Through analyzing all the Euler angles of α grains within a steel, then plotting the Euler angle in a three-dimensional graph and calculating the probability density function, the above ODF maps can be made. It can be seen from ODF maps that the maximum orientation intensity is only 1.22 times greater than the random equivalent, which indicates that there is no preferential orientation in the 3Mn steel. Similarly, ODF maps of 5Mn and 7Mn steels were also calculated, and the results also indicated that there is no preferential orientation in the steel. The results of the ODF maps correspond with the IPF maps in Figure 5. Since there is no preferential orientation in three steels, it can be deduced that completely dynamic recrystallization takes place during their warm deformation processes.

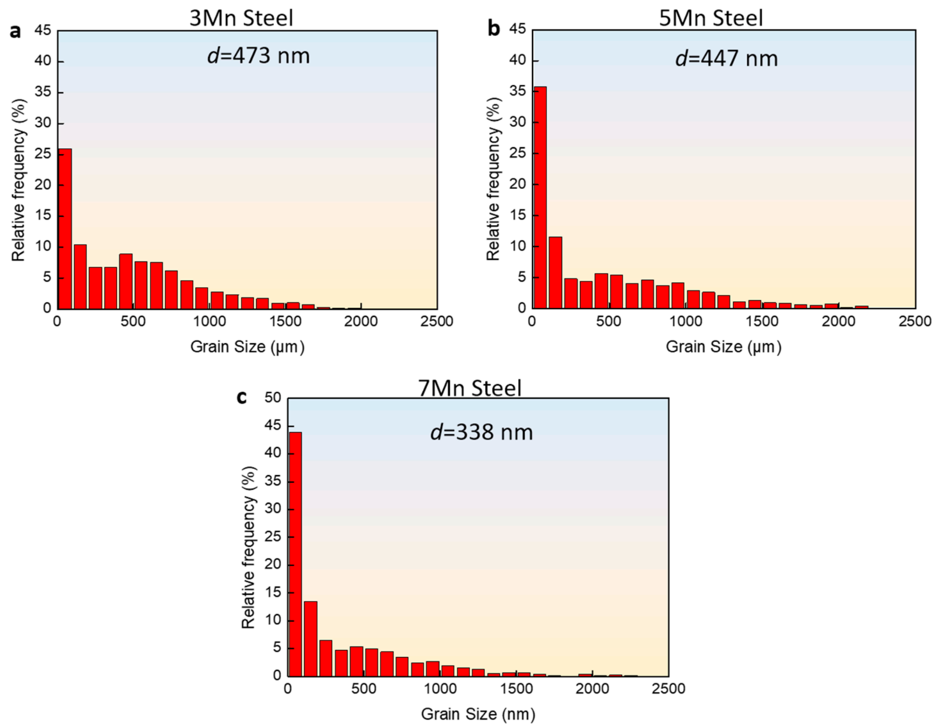

Figure 5. Grain size distribution maps of the α phase in three experimental steels: (**a**) 3Mn steel; (**b**) 5Mn steel; (**c**) 7Mn steel.

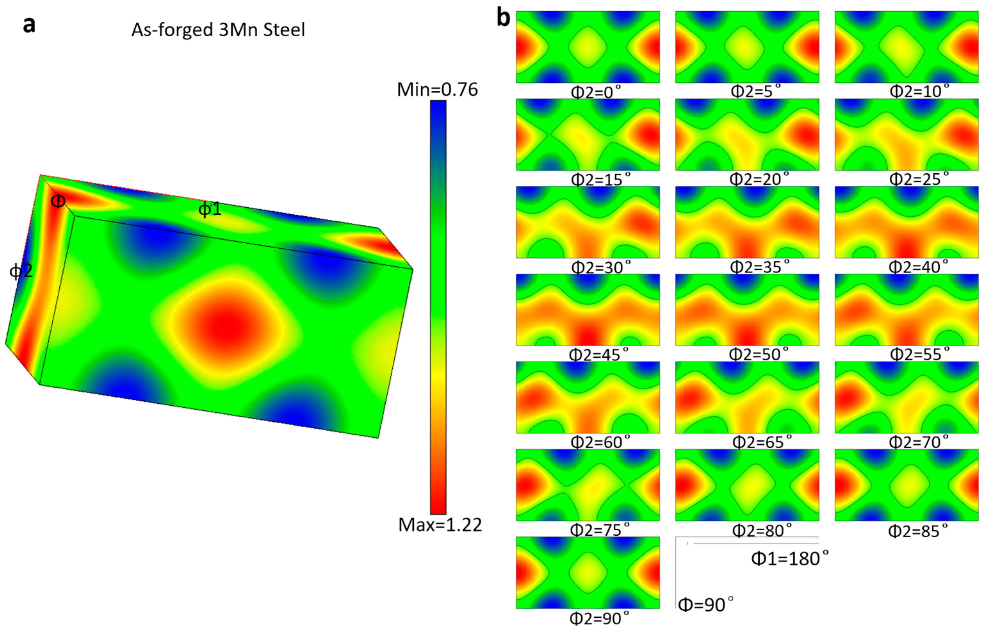

Figure 6. The α phase orientation distribution function (ODF) map of the as-forged 3Mn steel: (**a**) three-dimensional ODF map; (**b**) cross-section views of figure (**a**) with an interval of Φ2 = 5°.

3.4. Mechanical Properties of As-Forged Steels

Figure 7a shows the room-temperature tensile curves of the three as-forged steels. The tensile strengths of the three steels range between 1.9 and 2.1 GPa, and their elongations range between 7 and 8.5%. The yield strengths of the three steels significantly decrease as the manganese content increases. This is because the area fraction of the γ phase increases as the manganese content increases (Figure 4). Since the Peierls–Nabarro stress of the γ phase is lower than that of the α phase, increasing the area fraction of the γ phase results in a lower yield strength [22,23]. A comparison of the tensile properties between the three steels in this study and other steels reported in the literature is shown in Figure 7b [1–7,9,12–14]. The advantage of the present three steels is that they have higher strengths without significant decreases in ductility. This result can be attributed to the following three reasons: First, grain refinement is not only beneficial for impeding the motion of dislocations, thus improving the materials' strengths; it is also beneficial for improving the coordination between grains, thus enhancing the ductility of the materials [24]. Second, dislocations can be annihilated during warm deformation, and a decrease in dislocation density would increase the mobility of dislocations, thereby improving the ductility of the material as well. Third, the TRIP effect also contributes to higher ductility [1,2,7].

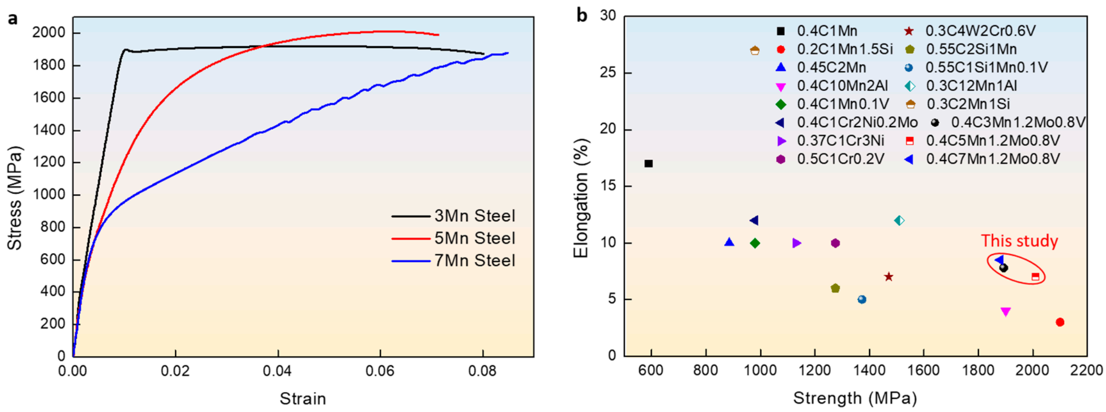

Figure 7. Room-temperature tensile properties of the three steels: (**a**) room-temperature tensile curves; (**b**) the elongation–strength scatter diagram.

To demonstrate that the TRIP effect was a significant deformation mechanism of the three steels, microstructures near the fracture surfaces after the tensile tests were characterized using EBSD. The results are shown in Figure 8. Compared with the microstructures before the tensile tests (Figure 4), both the α grain sizes and the preferential orientation characteristics are barely changed; however, the area fractions of the γ phases have decreased, indicating that the $\gamma \rightarrow \alpha'$ phase transformation takes place during the tensile tests. Through using EBSD analysis software Channel 5.0, the area fraction of γ phase in the steel was quantitatively measured, as shown in Figure 9. In the 3Mn steel, the area fraction of the γ phase decreased from 0.74 $\pm$ 0.05% to 0.12 $\pm$ 0.01% after the tensile test. In the 5Mn steel, the area fraction of the γ phase decreased from 8.84 $\pm$ 0.84% to 2.74 $\pm$ 0.33% after the tensile test. In the 7Mn steel, the area fraction of the γ phase decreased from 24.6 $\pm$ 1.33% to 8.7 $\pm$ 0.45% after the tensile test. It can be seen that among the three investigated steels, the area fraction of the γ phase in the 7Mn steel decreased most significantly after the tensile test; hence, the TRIP effect in this steel plays a more important role than in the other two investigated steels. It can be seen that the tensile curve of the 7Mn steel fluctuates at high strain (Figure 7). It also undergoes significant hardening, which would suppress necking in the material. This explains why the 7Mn steel has the highest elongation of the three investigated steels [3–6].

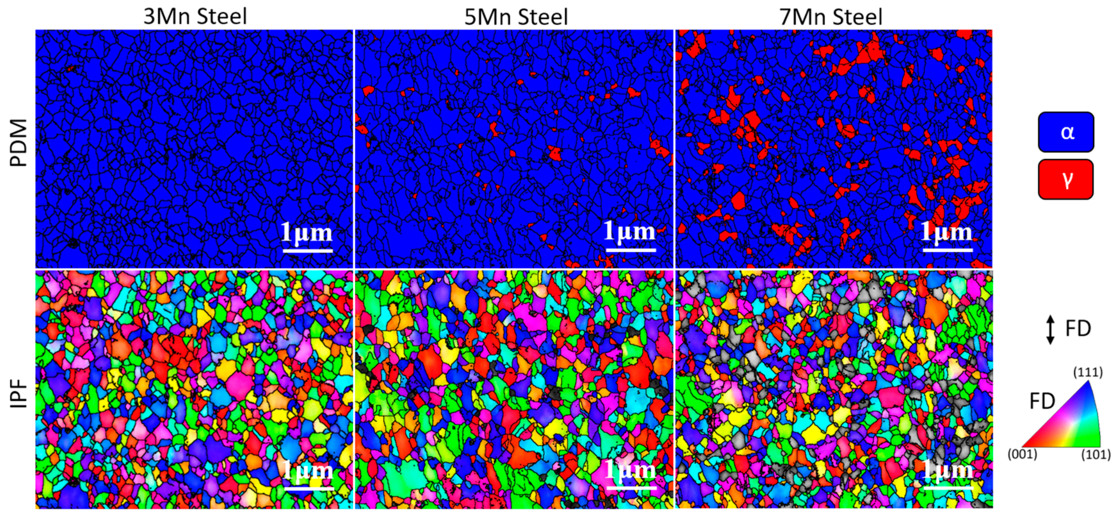

Figure 8. EBSD microstructures of the three steels after tensile tests; the forging direction (FD) is labelled on the right.

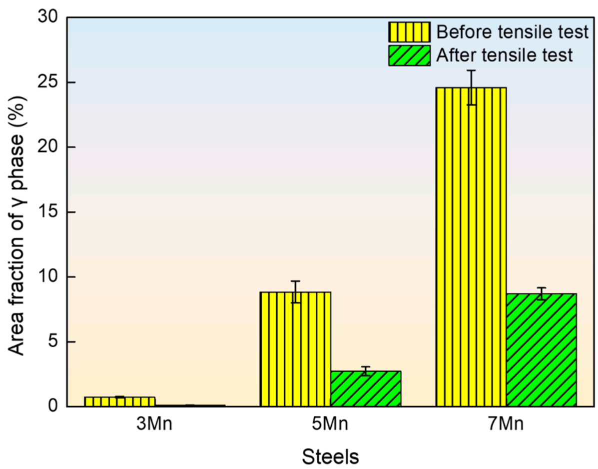

Figure 9. Area fraction of the γ phase in three experimental steels before and after tensile tests.

3.5. Microstructural Thermostability of Ultrafine-Grained Steels

Although the ultrafine-grained steels in this study are of high strength, the high number of grain boundaries in steels also provided a strong diving force for grain coarsening [25–28]. Once grain coarsening takes place, the steels will lose their high mechanical performance [28]. Therefore, it is imperative to conduct thermal exposure experiments so as to evaluate the microstructural thermostability of the three ultrafine-grained steels. Figure 10 shows the changes in the hardness of the three steels after thermal exposure at 100~600 °C for 1 h. It can be seen that when the exposure temperature is within a range of 100~200 °C, the hardness of all three steels decreases slightly (no more than 2%) compared with their as-forged state. As grain coarsening is impossible at such lower temperatures, it is reasonably deduced that vacancy or dislocation annihilation during the thermal exposure process results in the hardness decreasing. When the thermal exposure temperature increases to the range of 300~400 °C, the hardness of all three steels abnormally increases with the increase in temperature. This phenomenon should be related to the V and Mo alloyed in the steels; the precipitation of VC, MoC, or Mo_2C carbides during the thermal exposure process would contribute to the role of secondary hardening [29,30]. When the thermal exposure temperature increases to 500 °C, the hardness of 3Mn steel and 5Mn steel still increases with the increase in temperature, which hints that more VC, MoC, or Mo_2C carbides precipitate from their matrix, and they are contributing to a more prominent role of secondary hardening. While the hardness of the 7Mn steel decreases with the increase in temperature, this indicates the ultrafine-grained microstructure is on the verge of losing thermostability. When the thermal exposure temperature further increases to 600 °C, only the 3Mn steel is of a similar hardness to its initial as-forged state, demonstrating that the ultrafine-grained microstructure of the steel has a high level of thermostability. The hardness of the 5Mn steel decreases from 605 ± 9 kgf/mm^2 to 581 ± 8 kgf/mm^2, and its microstructural thermostability is inferior to the 3Mn steel; while the hardness of the 7Mn steel significantly decreases from an initial 579 ± 8 kgf/mm^2 to 523 ± 7 kgf/mm^2, demonstrating that the ultrafine-grained microstructure of the 7Mn steel has the lowest thermostability among the three steels. Based on the above result, it can be seen that the microstructural thermostability of experimental steels decreases with the increase in Mn content. This phenomenon can be attributed to the following reasons: On the one hand, the alloying of Mn in steels would decrease the Ac1 temperature, which would promote the α phase transforming into the γ phase when it is exposed at high temperatures; thus, Mn alloying would decrease the microstructure thermostability. On the other hand, the alloying of Mn in steels would increase the self-diffusional coefficient of both the α and γ phases, which promotes grain boundary migration during the thermal exposure process [31,32]. Therefore, Mn alloying would decrease the microstructural thermostability of the steel [3,33,34].

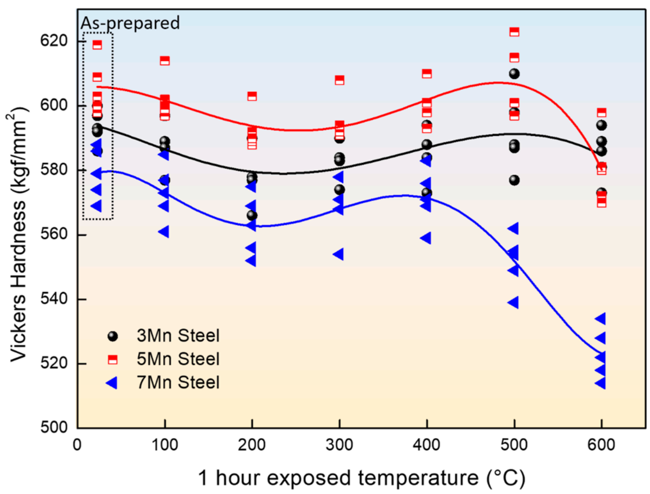

Figure 10. Changes in the hardness of three experimental steels after exposure at 100~600 °C for 1 h.

4. Conclusions

In this study, by using warm deformation at the (α + γ) dual-phase region, we have successfully fabricated 0.4C-(3, 5, 7)Mn-1.2Mo-0.8V TRIP steels with ultrafine-grained microstructures. The main conclusions are as follows:

(1) The warm deformation flow stresses of the three steels range between 500 and 750 MPa, which are much lower than those of conventional TRIP steels. Ultrafine-grained microstructures with average α grain sizes of 200–500 nm were fabricated after the warm deformations.

(2) As the Mn content increases, the Ac1, Ac3 and Ms temperatures of the three investigated steels gradually decrease, and the area fraction of the γ phase increases after warm deformation.

(3) The tensile strengths of the three investigated steels range between 1.9 and 2.1 GPa, and the elongations range between 7% and 8.5%. The good mechanical properties of the steels can be attributed to both grain refinement and the TRIP effect.

(4) The microstructural thermostability of three experimental steels decreases with the increase in Mn content; the 3Mn steel demonstrates high microstructural thermostability even after thermal exposure at 600 °C for 1 h.

Author Contributions: Conceptualization, H.W. and L.R.; Methodology, K.K., X.R., P.Z., S.Z., Y.L., H.L. (Huan Liu), K.Y. and H.Y.; Formal analysis, H.W.; Investigation, X.R., S.Z., Y.L. and H.L.; Data curation, H.W., P.Z., Y.L., H.L. (Hui Liu), K.Y. and H.Y.; Writing—original draft, J.Z. and K.K.; Supervision, L.R., H.Y. and K.Y. All authors have read and agreed to the published version of the manuscript.

Funding: This work was financially supported by the National Key Research and Development Program of China (2022YFB3705203, 2022YFC2406003, 2022YFC2406001), the Bintech-IMR R&D Program (GYY-JSBU-2022-008), the IMR Innovation Fund (2023-PY06), the Foundation of Shenyang University of Chemical Technology (No. LJ2020011), and the Natural Science Foundation of Liaoning (2023-MS-022).

Data Availability Statement: All data are available in the main text.

Conflicts of Interest: The authors declare no conflict of interest.

References

1. Liu, S.; Qian, L.; Meng, J.; Li, D.; Ma, P.; Zhang, F. Simultaneously increasing both strength and ductility of Fe-Mn-C twinning-induced plasticity steel via Cr/Mo alloying. *Scr. Mater.* **2017**, *127*, 10–14. [CrossRef]
2. Yang, H.K.; Tian, Y.Z.; Zhang, Z.J.; Zhang, Z.F. Simultaneously improving the strength and ductility of Fe-22Mn-0.6C twinning-induced plasticity steel via nitrogen addition. *Mater. Sci. Eng. A Struct. Mater. Prop. Misrostruct. Process.* **2018**, *715*, 276–280. [CrossRef]
3. Yang, D.P.; Du, P.J.; Wu, D.; Yi, H.L. The microstructure evolution and tensile properties of medium-Mn steel heat-treated by a two-step annealing process. *J. Mater. Sci. Technol.* **2021**, *75*, 205–215. [CrossRef]
4. Danilov, V.I.; Orlova, D.V.; Gorbatenko, V.V.; Danilova, L.V.; Zuev, L.B. Kinetics of strain-induced phase transformation in TRIP steel. *Mater. Lett.* **2021**, *301*, 130289. [CrossRef]
5. Han, D.; Xu, Y.; Zhang, J.; Peng, F.; Sun, W. Relationship between crystallographic orientation, microstructure characteristic and mechanical properties in cold-rolled 3.5Mn TRIP steel. *Mater. Sci. Eng. A Struct. Mater. Prop. Misrostruct. Process.* **2021**, *821*, 141625. [CrossRef]
6. Ren, P.; Chen, X.P.; Wang, C.Y.; Zhou, Y.X.; Cao, W.Q.; Liu, Q. Evolution of microstructure, texture and mechanical properties of Fe–30Mn–11Al–1.2C low-density steel during cold rolling. *Mater. Charact.* **2021**, *174*, 111013. [CrossRef]
7. Zhang, B.; Zhao, M.M.; Dong, Y.; Misra, R.D.K.; Du, Y.; Wu, H.Y.; Du, L.X. On the structure-property relationship in a novel 1000 MPa hot-rolled TRIP steel with strain-assisted ferrite transformation. *Mater. Sci. Eng. A* **2021**, *821*, 141594. [CrossRef]
8. Jabońska, M.; Niewielski, G.; Kawalla, R. High Manganese TWIP Steel-Technological Plasticity and Selected Properties. *Solid State Phenom.* **2014**, *212*, 87–90. [CrossRef]
9. Wang, T.; Qian, L.; Li, K.; Zhang, F.; Meng, J. Strain-hardening behavior and mechanisms of a lamellar-structured low-alloy TRIP steel. *Mater. Sci. Eng. A* **2021**, *819*, 141498. [CrossRef]
10. Liu, C.; Peng, Q.; Xue, Z.; Wang, S.; Yang, C. Microstructure and Mechanical Properties of Hot- Rolled and Cold-Rolled Medium-Mn TRIP Steels. *Materials* **2018**, *11*, 2242. [CrossRef]
11. Kozowska, A.; Radwański, K.; Matus, K.; Samek, L.; Grajcar, A. Mechanical stability of retained austenite in aluminum-containing medium-Mn steel deformed at different temperatures. *Arch. Civ. Mech. Eng.* **2021**, *21*, 19. [CrossRef]
12. Li, J.; Zhang, F. A simultaneously improved strength and ductility on medium Mn TRIP steel designed by pre-twinning strategy based on SFE controlling. *Mater. Lett.* **2022**, *316*, 132078. [CrossRef]
13. Huang, C.; Huang, M. Effect of Processing Parameters on Mechanical Properties of Deformed and Partitioned (D&P) Medium Mn Steels. *Metals* **2021**, *11*, 356. [CrossRef]
14. Gao, B.; Lai, Q.; Cao, Y.; Hu, R.; Xiao, L.; Pan, Z.; Liang, N.; Li, Y.; Sha, G.; Liu, M.; et al. Ultrastrong low-carbon nanosteel produced by heterostructure and interstitial mediated warm rolling. *Sci. Adv.* **2020**, *6*, eaba8169. [CrossRef]
15. Wang, H.; Gao, W.; Zhang, X.; Li, Y.; Zhang, S.; Ren, L.; Yang, K. Enhanced Corrosion Resistance and Biological Properties of Ultrafine-Grained Ti15Zr5Cu Alloy. *Metals* **2022**, *12*, 1144. [CrossRef]
16. Li, D.; Qian, L.; Wei, C.; Liu, S.; Zhang, F.; Meng, J. The role of Mn on twinning behavior and tensile properties of coarse- and fine-grained Fe-Mn-C twinning-induced plasticity steels. *Mater. Sci. Eng. A Struct. Mater. Prop. Misrostruct. Process.* **2020**, *789*, 139586. [CrossRef]
17. Wang, X.-S.; Narayana, P.L.; Maurya, A.K.; Kim, H.-I.; Hur, B.-Y.; Reddy, N.S. Modeling the quantitative effect of alloying elements on the Ms temperature of high carbon steel by artificial neural networks. *Mater. Lett.* **2021**, *291*, 129573. [CrossRef]
18. Doherty, R.D.; Hughes, D.A.; Humphreys, F.J.; Jonas, J.J.; Jensen, D.J.; Kassner, M.E.; King, W.E.; McNelley, T.R.; McQueen, H.J.; Rollett, A.D. Current issues in recrystallization: A review. *Mater. Sci. Eng. A* **1997**, *238*, 219–274. [CrossRef]
19. Gao, W.; Wang, H.; Koenigsmann, K.; Zhang, S.; Ren, L.; Yang, K. Fabrication of ultrafine-grained Ti-15Zr-xCu alloys through martensite decompositions under thermomechanical coupling conditions. *J. Mater. Sci. Technol.* **2022**, *127*, 19–28. [CrossRef]
20. Wang, H.; Yan, W.; van Zwaag, S.; Shi, Q.; Wang, W.; Yang, K.; Shan, Y. On the 650 °C thermostability of 9–12Cr heat resistant steels containing different precipitates. *Acta Mater.* **2017**, *134*, 143–154. [CrossRef]

21. He, B.B.; Hu, B.; Yen, H.W.; Cheng, G.J.; Wang, Z.K.; Luo, H.W.; Huang, M.X. High dislocation density–induced large ductility in deformed and partitioned steels. *Science* **2017**, *357*, 1029–1032. [CrossRef]
22. Jeong, C.Y.; Nam, S.W.; Ginsztler, J. Activation processes of stress relaxation during hold time in 1Cr-Mo-V steel. *Mater. Sci. Eng. A* **1999**, *264*, 188–193. [CrossRef]
23. Mohammed, A.S.K.; Celebi, O.K.; Sehitoglu, H. Critical stress prediction upon accurate dislocation core description. *Acta Mater.* **2022**, *233*, 117989. [CrossRef]
24. Wang, H.; Song, W.; Liu, M.; Zhang, S.; Ren, L.; Qiu, D.; Chen, X.-Q.; Yang, K. Manufacture-friendly nanostructured metals stabilized by dual-phase honeycomb shell. *Nat. Commun.* **2022**, *13*, 2034. [CrossRef]
25. Song, W.; Wang, H.; Koenigsmann, K.; Zhang, S.; Ren, L.; Yang, K. Biomedical core–shell micro-nanocrystalline Ti6Al4V5Cu alloy with high fatigue properties. *Mater. Des.* **2023**, *227*, 111769. [CrossRef]
26. Chao, Q.; Hodgson, P.D.; Beladi, H. Thermal stability of an ultrafine grained Ti-6Al-4V alloy during post-deformation annealing. *Mater. Sci. Eng. A* **2017**, *694*, 13–23. [CrossRef]
27. Chookajorn, T.; Murdoch, H.A.; Schuh, C.A. Design of Stable Nanocrystalline Alloys. *Science* **2012**, *337*, 951. [CrossRef]
28. Hu, J.; Shi, Y.N.; Sauvage, X.; Sha, G.; Lu, K. Grain boundary stability governs hardening and softening in extremely fine nanograined metals. *Science* **2017**, *355*, 1292. [CrossRef]
29. Sawada, K.; Kubo, K.; Abe, F. Creep behavior and stability of MX precipitates at high temperature in 9Cr–0.5Mo–1.8W–VNb steel. *Mater. Sci. Eng. A* **2001**, *319*, 784–787. [CrossRef]
30. Klueh, R.L.; Alexander, D.J.; Sokolov, M.A. Effect of chromium, tungsten, tantalum, and boron on mechanical properties of 5–9Cr–WVTaB steels. *J. Nucl. Mater.* **2002**, *304*, 139–152. [CrossRef]
31. Stechauner, G.; Kozeschnik, E. Self-Diffusion in Grain Boundaries and Dislocation Pipes in Al, Fe, and Ni and Application to AlN Precipitation in Steel. *J. Mater. Eng. Perform.* **2014**, *23*, 1576–1579. [CrossRef]
32. Inoue, A.; Nitta, H.; Iijima, Y. Grain boundary self-diffusion in high purity iron. *Acta Mater.* **2007**, *55*, 5910–5916. [CrossRef]
33. Wang, K.; Tan, Z.; Gao, G.; Gao, B.; Gui, X.; Misra, R.D.; Bai, B. Microstructure-property relationship in bainitic steel: The effect of austempering. *Mater. Sci. Eng. A* **2016**, *675*, 120–127. [CrossRef]
34. Jeya Ganesh, B.; Raju, S.; Kumar Rai, A.; Mohandas, E.; Vijayalakshmi, M.; Rao, K.B.S.; Raj, B. Differential scanning calorimetry study of diffusional and martensitic phase transformations in some 9 wt-%Cr low carbon ferritic steels. *Mater. Sci. Technol.* **2013**, *27*, 500–512. [CrossRef]